Stator ITSC Fault Diagnosis for EMU Induction Traction Motor based on Goertzel Algorithm and Random Forest

Jie Ma , Yingxue Li , Liying Wang , Jisheng Hu , Hua Li , Jiyou Fei * , Lin Li , Geng Zhao

Posted Date: 23 May 2023

doi: 10.20944/preprints202305.1623.v1

Keywords: Goertzel algorithm; ITSC fault; traction motor; random forest; fault diagnosis

Article

Stator ITSC Fault Diagnosis for EMU Induction Traction Motor based on Goertzel Algorithm and Random Forest

Jie Ma [1,2], Yingxue Li [1], Liying Wang [1], Jisheng Hu [1], Hua Li [1], Jiyou Fei [1,*], Lin li [1], Geng Zhao [1]

[1] College of Locomotive and Rolling Stock Engineering, Dalian Jiaotong University, Dalian 116028, China; majie@lntdxy.com (J.M.); liyingxue@djtu.edu.cn (Y.L.); wangly@djtu.edu.cn (L.W.); bssmd@126.com (J.H.); lihua@djtu.edu.cn (H.L.); lilin_dljt@djtu.edu.cn (L.L.);zhaogeng1983@163.com (G.Z.)

[2] Liaoning Railway Vocational and Technical College, Jinzhou 121000, China;

* Correspondence: fjy@djtu.edu.cn

Abstract: The stator winding insulation system is the most critical and weak part of the EMU's (electric multiple unit) traction motor. The effective diagnosis for stator ITSC (inter-turn short-circuit) faults can prevent the fault from expanding into phase-to-phase or ground short-circuits. The TCU(traction control unit) controls the traction inverter to output SPWM (sine pulse width modulation) excitation voltage when the traction motor is stationary. Three ITSC fault diagnostic conditions are based on different IGBTs control logic. The Goertzel algorithm is used to calculate the fundamental current amplitude difference Δi and phase angle difference $\Delta\theta$ of equivalent parallel windings under the three diagnostic conditions. The six parameters under the three diagnostic conditions are used as features to establish an ITSC fault diagnostic model based on random forest. The proposed method was validated using a simulation experimental platform for ITSC fault diagnosis of EMU traction motors. The experimental results indicate that the current amplitude features Δi and phase angle features $\Delta\theta$ change obviously with the increase of ITSC fault extent if the ITSC fault occurs at the equivalent parallel windings. The accuracy of the ITSC fault diagnosis model based on the random forest for ITSC fault detection and location both in train and test samples are 100%.

Keywords: Goertzel algorithm; ITSC fault; traction motor; random forest; fault diagnosis

1. Introduction

The EMUs' electric drive system generally adopts AC drive mode, and the AC induction motors are used for electromechanical energy conversion. As the core energy conversion component, traction motors play a crucial role in the EMUs' normal operation[1]. Due to reliable operation and convenient maintenance, three-phase squirrel cage induction motors are still the main form of traction motors[2]. The insulation system is the "heart" of the traction motor. The traction motor is powered by a traction converter, and the inverter generally uses SVPWM (space vector pulse width modulation) and square wave power supply to the traction motor for different control stages[3,4].The stator ITSC fault of the induction motor accounts for 37% in industry application, and it is more destructive than rotor bar breakage, air gap eccentricity, and bearing faults [5,6]. Due to the effect of the SVPWM voltage pulses supplied by the inverter, the traction motor bears greater voltage stress and is also affected by thermal stress and environmental factors, the ITSC fault is more prominent . If the ITSC fault can be accurately diagnosed during the incipient stage, it can be avoided to expand into ground short-circuit or phase-to-phase short-circuit faults while saving maintenance costs. The accurate ITSC fault diagnosis can provide a reference for the traction motor state-based repair. Current, diagnosis methods for stator ITSC faults in induction motors mainly include model based fault diagnosis, signal analysis based fault diagnosis, and artificial intelligence based fault diagnosis.

The model-based diagnosis for ITSC fault mainly includes two approaches: state variable observation and parameter estimation methods. A coordinate transformation theory was used to obtain a dynamic model of an induction motor with the ITSC fault and convert the model into a state equation form which is amenable to numerical simulation[7]. The negative sequential current value of an induction motor was estimated from this model to determine the ITSC fault degree. A mathematical model of the induction motor with stator ITSC fault was established, and an adaptive observer was designed using this model[8]. The observer can estimate the stator inter-turn insulation state under voltage imbalance and speed change conditions. This diagnosis method can be applied to the grid and converter supply conditions. A new stator ITSC fault detection method was proposed based on the model [9]. The state observer was used to generate a specific residual vector. This approach allows rapid monitoring of ITSC faults at the initial stage. To compensate for the impact of non-equilibrium supply voltage and the existing asymmetry of the three-phase windings. A new stator ITSC fault model for the induction motor was proposed[10]. This model can accurately determine the ITSC fault extent and location. The motor models were established with ITSC fault related parameters, and the motor faults can be diagnosed by identifying the fault parameters[11-13]. The genetic algorithm was used to estimate the basic parameters of the motor, including the stator and rotor resistance, the self inductance and mutual inductance, and the number of turns in the short-circuit phase[14]. These parameters are closely related to the stator ITSC fault.

Signal-based diagnostic methods for ITSC faults mainly use traditional FFT transform, power spectrum analysis, and modern time-frequency analysis to detect the ITSC faults. After the outage, the ITSC fault was diagnosed by detecting the third harmonic component value in the residual voltage. This method is not affected by motor parameters and power supply imbalance [15]. The stator ITSC fault in a three-phase induction motors was diagnosed by analyzing the third harmonic component in the positive and negative sequence currents[16]. A new method for parameter spectrum estimation was proposed, which can take the advantage of fault sensitive frequencies and obtain high-precision frequencies using the maximum likelihood estimation method[17]. The lower sideband of the power supply frequencies were analyzed, and the Kalman Filter was used to estimate the harmonic amplitude[18]. The total distortion of instantaneous harmonic current in each phase was used as the fault judgment criterion. If the amplitude at a certain phase exceeds a predetermined threshold, it is determined that the ITSC fault has occurred. Discrete wavelet or wavelet packet transform was used to analyze the current value, power spectral density, and other parameters[19-24]. Parameters such as the energy ratio of a particular frequency band were used for fault diagnosis in the induction motors. In addition to the wavelet method, time-frequency analysis methods such as EMD (empirical mode decomposition) can also be applied to diagnose stator ITSC faults in induction motors [25]..

Artificial intelligence methods for ITSC fault diagnosis in induction motor stators mainly used intelligent pattern recognition methods such as neural networks to evaluate and locate the ITSC faults [26-28]. The energy ratio of the three-phase current frequency bands calculated with the discrete wavelet transform was taken as the fault features. The Bayesian regularization Elman network is a fault diagnosis model, which can achieve high accuracy in ITSC fault detection and location at the ITSC incipient stage[29]. A HCNN (hierarchical convolution neural network) with a two-layer hybrid structure and a SVM (support vector machine) algorithm was proposed to diagnose induction motor incipient ITSC faults. The HCNN network identified stator fault modes and extracted fault features, and the SVM evaluated the fault extent [30]. The random forest and XGBoost were used to diagnose mixed faults. A two-phase current was filtered and used as the diagnostic signal. The wavelet packet decomposition was used to extract fault features, and finally, PCA (principal component analysis) was used to reduce the fault features dimensions. This method took a CRH2(china railway high-speed) traction motor as the diagnostic object and proved its effectiveness through a semi-physical simulation system[31].

Although there are more and more research achievements in industrial induction motors for stator ITSC diagnosis, there are specific requirements for the EMU's induction traction motors ITSC fault diagnosis. In the case of converter power supply, closed-loop control, and complex harmonics,

 doi:10.20944/preprints202305.1623.v1

the ITSC faults diagnosis for traction motors is still an open problem [32]. Diagnostic methods for stator winding based on the fault signals such as negative sequence current components, zero sequence voltage, and high order current harmonics are essential to detect asymmetries in three-phase winding. This article proposed a method of controlling the traction inverter IGBTs to detect the asymmetry of the three-phase winding under the traction motor stationary state. The traction converter is used to output the SPWM excitation voltage. According to the different IGBTs control logic, three ITSC fault diagnostic conditions exist. The Goertzel algorithm is used to calculate the fundamental current amplitude difference Δi and phase angle difference $\Delta\theta$ of equivalent parallel windings under diagnostic conditions. The fundamental amplitude difference Δi and phase angle difference $\Delta\theta$ of equivalent parallel windings under three diagnostic conditions are used as fault features. The random forest is used to establish the traction motor ITSC fault diagnosis model. After training, the ITSC fault detection and location model based on the random forest can detect the traction motor ITSC fault and locate the ITSC fault (a, b, c phase windings). The extent of ITSC fault can also be evaluated according to the fault features. This method can be achieved by utilizing only the existing current sensors in the traction system, without additional sensors, and is a non-invasive fault diagnosis method. The ITSC faults are detected in the stationary state of the traction motor, and the diagnosis is not affected by other faults such as rotor bar breakage and air gap eccentricity. The ITSC fault diagnosis method proposed in this article for traction motors in a stationary state has a stable fault diagnosis environment. The diagnosis process is unaffected by load and speed, making the diagnosis more accurate and reliable.

The article consists of six sections. After the introduction of the current method used for ITSC fault diagnosis in industry, a brief introduction of the new diagnosis method for the EMUs' traction motors was presented. The traction motor stator ITSC fault diagnostic condition control method was presented in Section 2, the TCU controlled the traction inverter to work in three diagnostic conditions. The SPWM excitation voltage control and the Goertzel algorithm were presented in Section 3, the frequency and modulation index of SPWM excitation voltage were set, and the Goertzel algorithm was used to compute the amplitude and phase angle of three-phase current fundamental component. The fault features extraction method and the random forest model were presented in Section 4, the flowchart of the new method for ITSC fault diagnosis was also presented in this section. In Section 5, the EMU traction motor ITSC simulation experimental platform and the signals measurement system were described, the voltage and current signal of the platform were also analyzed in this section. The experimental results of the stator ITSC fault method based on Goertzel algorithm and random forest were given, the comparisons with other machine leaning algorithm in accuracy were also presented in Section 5. The paper is concluded with a short summary.

2. Traction Motor Stator ITSC Fault Diagnostic Condition Control

Figure 1 shows the structural diagram of the EMU traction system, which mainly consists of a 4-quadrant rectifier, a DC-link, a traction inverter and traction motors. The 4-quadrant rectifier rectifies the 25kV/50Hz single-phase AC pulled in by the pantograph into DC, and the DC link mainly includes a second harmonic filter circuit and support capacitors. The traction inverter inverts DC voltage into a three-phase VVVF (variable frequency variable voltage) AC power supply to drive the traction motor to operate. The TCU primarily controls the EMU traction system.

Preprints (www.preprints.org) | NOT PEER-REVIEWED | Posted: 23 May 2023 doi:10.20944/preprints202305.1623.v1

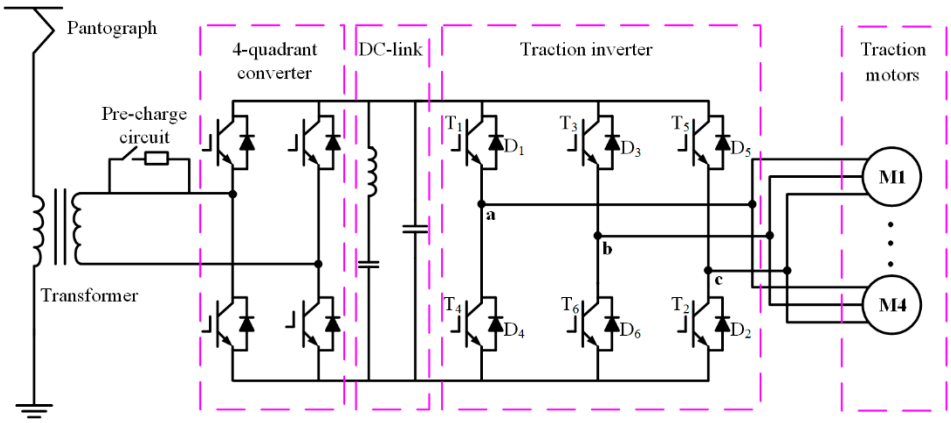

Figure 1. Structural diagram of the EMU traction system.

2.1. Working Status of Two-level Traction Inverter

The main circuit topology of the two-level traction inverter is shown in Figure 1, which mainly consists of six IGBTs, T_1, T_2, T_3, T_4, T_5 and T_6, forming a three-phase full bridge inverter circuit. For the convenience of analysis, three ideal switching functions are usually defined [6]: S_A={1-T_1 switch on; 0-T_4 switch on }, S_B={1-T_3 switch on; 0-T_6 switch on }, S_C={1-T_5 switch on; 0-T_2 switch on }. There are eight combinations of S_A, S_B and S_C, and their switch states in various modes are shown in Table 1.

Table 1. Working status of two-level traction inverter.

Mode	**0**	**1**	**2**	**3**	**4**	**5**	**6**	**7**
S_A	0	0	0	0	1	1	1	1
S_B	0	0	1	1	0	0	1	1
S_C	0	1	0	1	0	1	0	1
Voltagevector	$\overrightarrow{U_0}$	$\overrightarrow{U_1}$	$\overrightarrow{U_2}$	$\overrightarrow{U_3}$	$\overrightarrow{U_4}$	$\overrightarrow{U_5}$	$\overrightarrow{U_6}$	$\overrightarrow{U_7}$

2.2. ITSC Fault Diagnostic Condition Control

Traction motor ITSC fault diagnostic conditionIis shown in Figure 2. The driving signals of T_1, T_2 and T_6 are the same, and switched on and off simultaneously; the driving signals of T_3, T_4 and T_5 are the same, and switched on and off simultaneously. When T_1, T_2 and T_6 are switched on, and T_3, T_4 and T_5 are switched off simultaneously, this is equivalent to applying a voltage vector $\overrightarrow{U_4}$ to the traction motor; when T_3, T_4 and T_5 are switched on, and T_1, T_2 and T_6 switched off simultaneously, this is equivalent to applying a voltage vector $\overrightarrow{U_3}$ to the traction motor. The directions of the three currents i_a, i_b and i_c in Figure 2 represent the reference directions of the currents, not the actual flow directions. Suppose the IGBTs driving signals Ugs1, Ugs2, Ugs6, and Ugs3, Ugs4, Ugs5 drive the IGBTs in a bipolar sine pulse width modulation mode. The intermediate DC voltage applies single-phase SPWM voltages to the stator windings of the traction motor. Under diagnostic condition I, the b-phase winding and the c-phase winding of the traction motor are connected parallel and in series with the a-phase winding.

Preprints (www.preprints.org) | NOT PEER-REVIEWED | Posted: 23 May 2023 doi:10.20944/preprints202305.1623.v1

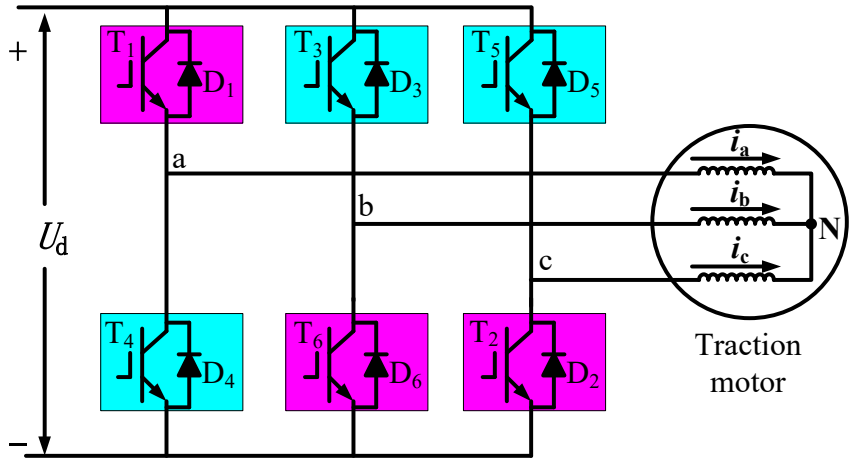

Figure 2. Diagnostic condition I inverter control.

Traction motor ITSC fault diagnostic condition II is shown in Figure 3. The driving signals of T_2, T_3 and T_4 are the same, and switched on and off simultaneously; the driving signals of T_1, T_5 and T_6 are the same and switched on and off simultaneously. When T_2, T_3 and T_4 are switched on, and T_1, T_5 and T_6 are switched off simultaneously, this is equivalent to applying a voltage vector $\overrightarrow{U_5}$ to the traction motor; when T_1, T_5 and T_6 are switched on, and T_2, T_3 and T_4 are switched off simultaneously, this is equivalent to applying a voltage vector $\overrightarrow{U_2}$ to the traction motor. The directions of three currents i_a, i_b, and i_c in Figure 3 represent the reference directions of the currents, not the actual flow directions. Suppose the IGBTs driving signals Ugs1, Ugs5, Ugs6, Ugs2, Ugs3, and Ugs4 drive the IGBTs in a bipolar sine pulse width modulation mode. The intermediate DC voltage applies single-phase SPWM voltages to the stator windings of the traction motor. Under diagnostic condition II, the a-phase winding and the c-phase winding of the traction motor are connected parallel and in series with the b-phase winding.

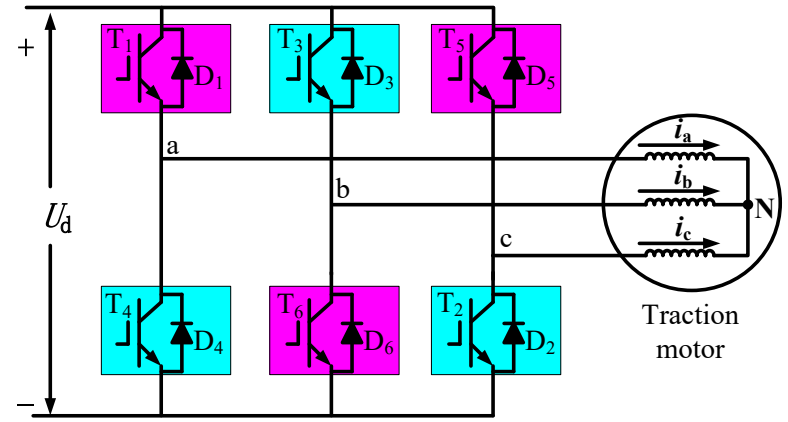

Figure 3. Diagnostic condition II inverter control.

Traction motor ITSC fault diagnostic condition III is shown in Figure 4. The driving signals of T_1, T_2 and T_3 are the same, and switched on and off simultaneously; the driving signals of T_4, T_5 and T_6 are the same, and switched on and off simultaneously. When T_1, T_2 and T_3 are switched on, and T_4, T_5 and T_6 are switched off simultaneously, this is equivalent to applying a voltage vector $\overrightarrow{U_6}$ to the traction motor; when T_4, T_5 and T_6 are switched on, and T_1, T_2 and T_3 are switched off simultaneously, this is equivalent to applying a voltage vector $\overrightarrow{U_1}$ to the traction motor. The directions of three currents i_a, i_b and i_c in Figure 4 represent the reference directions of the currents, not the actual flow directions. Suppose the IGBTs driving signals Ugs1, Ugs2, Ugs3, Ugs4, Ugs5, and Ugs6 drive the

Preprints (www.preprints.org) | NOT PEER-REVIEWED | Posted: 23 May 2023 doi:10.20944/preprints202305.1623.v1

IGBTs in a bipolar sine pulse width modulation mode. The intermediate DC voltage applies single-phase SPWM voltages to the stator windings of the traction motor. Under diagnostic condition III, the a-phase winding and the b-phase winding of the traction motor are connected parallel and in series with the c-phase winding.

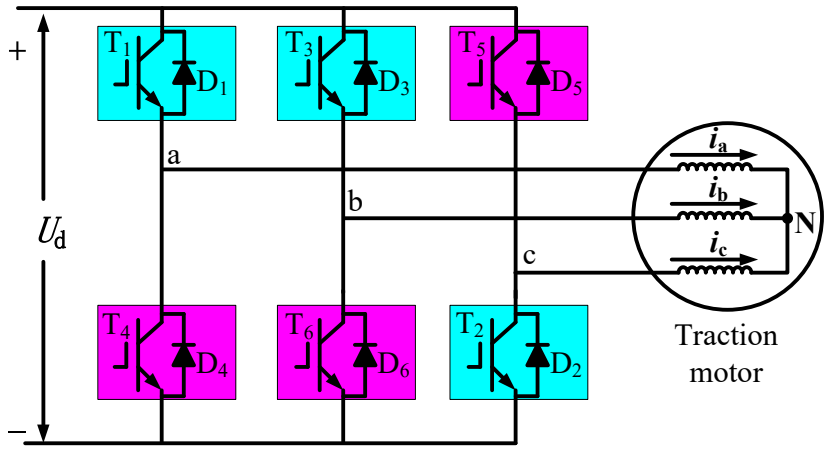

Figure 4. Diagnostic condition III inverter control.

2.3. Traction Motor Magnetomotive Force Analysis under Diagnostic Condition

Assuming that the traction motor is a complete symmetry motor, taking condition I as an example, the fundamental currents of the three-phase winding are:

$$\left.\begin{aligned} i_{a1} &= 2\sqrt{2}I_1 \cos wt \\ i_{b1} &= i_{c1} = -\sqrt{2}I_1 \cos wt \end{aligned}\right\} \quad (1)$$

In Formula(1), I_1 represents the fundamental RMS value of the b-phase and c-phase currents, and w represents the fundamental angular frequency of the SPWM excitation voltage.

The axes of the three-phase winding are separated by an electrical angle of 120° in space, and the fundamental magnetomotive forces of phases a, b, and c are:

$$\left.\begin{aligned} f_{a1} &= 2F_{p1} \cos wt \cos X \\ f_{b1} &= -F_{p1} \cos wt \cos(X - 120^\circ) \\ f_{c1} &= -F_{p1} \cos wt \cos(X - 240^\circ) \end{aligned}\right\} \quad (2)$$

The winding axis of the a-phase is taken to be the origin, and X represents the position of any point in the motor air gap. F_{p1} is the maximum amplitude of the fundamental magnetomotive forces, and its expression is:

$$F_{p1} = 0.9\frac{IN_s}{p}k_w \quad (3)$$

N_s is the number of series turns per phase of the stator winding, p is the number of pole pairs of the traction motor, and k_w is the winding coefficient of the fundamental magnetomotive force. The resultant magnetomotive force at any point in the air gap during fault diagnostic condition I is:

$$f_1 = f_{a1} + f_{b1} + f_{c1} = 2F_{p1}\cos wt \cos X - F_{p1}\cos wt \cos(X - 120^\circ) - F_{p1}\cos wt \cos(X - 240^\circ) = 3F_{p1}\cos wt \cos X \quad (4)$$

Preprints (www.preprints.org) | NOT PEER-REVIEWED | Posted: 23 May 2023 doi:10.20944/preprints202305.1623.v1

Formula(4) shows that when diagnostic condition I is applied to the traction motor, a pulsating magnetomotive force is generated in the traction motorair gap. Similarly, diagnostic conditions II and III also generate pulsating magnetomotive force, which does not generate a rotating magnetic field so that no electromagnetic torque will be generated, and the traction motor does not rotate.

3. SPWM Excitation Voltage and Goertzel Algorithm

3.1. Traction Motor SPWM Excitation Voltage Control

The EMU traction motors generally use separate cooling fans for cooling. Therefore, when the traction motor RMS current value is controlled to be less than the nominal current value in the stationary state, the motor should not cause damage to the traction motor due to heating. Under various diagnostic conditions, the bipolar SPWM voltage modulation method is used to output the ITSC fault diagnosis excitation voltage. The modulated wave is a sine wave with a triangular wave as the carrier. Select the appropriate modulation wave frequency f_r and carrier frequency f_c to determine the carrier ratio N:

$$N = \frac{f_c}{f_r} \tag{5}$$

Under various diagnostic conditions, the inverter operates in a single-phase full bridge inverter state, and the fundamental amplitude of the output voltage is:

$$U_{1m} = U_d \bullet M \tag{6}$$

where U_d is the DC link voltage, and M is the SPWM modulation index, which is defined as:

$$\mathrm{M} = \frac{U_{rm}}{U_{cm}} \tag{7}$$

In Formula(7), U_{rm} is the amplitude of the reference signal, and U_{cm} is the amplitude of the carrier signal. The fundamental RMS value of the maximum current in the three-phase winding should reach a certain value smaller than the rated current. By controlling and adjusting the inverter SPWM modulation index M through TCU, the modulation index M of the SPWM excitation voltage is determined.

3.2. Calculation of Current Fundamental Component Using Goertzel Algorithm

TCU sets the frequency of excitation voltage input for ITSC fault diagnosis, and the current fundamental frequency can be obtained accurately. Under the condition of knowing the exact current fundamental frequency, the current signals can be truncated throughout the entire cycle to avoid spectral leakage. The Goertzel algorithm can calculate only the amplitude and phase angle of the fundamental current component to reduce computational complexity and improve computational speed [33-36]. $x(n)$ is a sampling sequence of length N, $n \in [0, \text{N-1}]$, where n is an integer, then the DFT of $x(n)$ is:

$$X(k) = \sum_{n=0}^{N-1} x(n) W_N^{nk} \tag{8}$$

In Formula (8), taking $W_N = \mathrm{e}^{-j\frac{2\pi}{N}}$ into the following Formula to obtain:

$$W_N^{-kN} = \mathrm{e}^{\mathrm{j}2\pi k\,\mathrm{N}/\mathrm{N}} = \mathrm{e}^{\mathrm{j}2\pi k} = 1 \tag{9}$$

Multiply Formula(9) to the right of Formula(8):

$$X(k) = W_N^{-kN} \sum_{n=0}^{N-1} x(n) W_N^{kn} = \sum_{n=0}^{N-1} x(n) W_N^{-k(N-n)} \tag{10}$$

Preprints (www.preprints.org) | NOT PEER-REVIEWED | Posted: 23 May 2023 doi:10.20944/preprints202305.1623.v1

Define two sequences as:

$$x_e(n)=\begin{cases}x(n), & 0\leqslant n\leqslant N-1\\ 0, & else\end{cases} \tag{11}$$

$$h_k(n)=\begin{cases}W_N^{-kn}, & n\geqslant 0\\ 0, & n<0\end{cases} \tag{12}$$

Formula (10) can be expressed as the convolution of the two sequences:

$$y_k(n)=\sum_{l=0}^{N-1}x(l)W_N^{-k(n-l)}=x_e(n)*h_k(n) \tag{13}$$

Perform a *Z*-transform on Formula (13), where the Z-transform of $y_k(n)$ is $Y_k(z)$, the *Z*-transform of $x_e(n)$ is $X_k(z)$, and the *Z*-transform of $h_k(n)$ is $H_k(z)$. The time-domain convolution of the two sequences is equal to the frequency domain multiplication. From Formula(12), it can be obtained:

$$H_k(z)=\frac{1}{1-W_N^{-k}z^{-1}} \tag{14}$$

Multiply $\left(1-W_N^k z^{-1}\right)$ the numerator and denominator of Formula(14) simultaneously:

$$H_k(z)=\frac{1-W_N^k z^{-1}}{\left(1-W_N^{-k}z^{-1}\right)\left(1-W_N^k z^{-1}\right)}=\frac{1-W_N^k z^{-1}}{1-2\cos(2\pi k/N)z^{-1}+z^{-2}} \tag{15}$$

The corresponding filter structure is shown in Figure 5, and the input-output relation of the filter is as follows:

$$\left.\begin{aligned}v_k(n)&=2\cos(2\pi k/N)v_k(n-1)-v_k(n-2)+x(n)\\ y_k(n)&=v_k(n)-W_N^k v_k(n-1)\end{aligned}\right\} \tag{16}$$

The filter output $y_k(N)$ in Figure 5 is the transformation coefficient $X(k)$ of the *N*-point DFT at point *k*. If it is necessary to calculate the amplitude and phase angle of a specific frequency, the corresponding k value is:

$$\frac{k}{N}=\frac{f_{\text{int}}}{f_s} \tag{17}$$

Calculate the amplitude and phase of a specific frequency find using Goertzel as shown in Formulas (18) and (19):

$$|y(N)|^2=v^2(N-1)+v^2(N-2)-2\cos\left(\frac{2\pi k}{N}\right)v(N-1)\ v(N-2) \tag{18}$$

$$\theta=\arg\{y(N)\}=\arctan\frac{\sin(2\pi k/N)\cdot v(N-2)}{v(N-1)-\cos(2\pi k/N)\cdot v(N-2)} \tag{19}$$

Figure 5 shows that the Goertzel algorithm can calculate a $y_k(n)$ for every $x(n)$ collected. Data collection and computation can be carried out simultaneously, overcoming the disadvantage of DFT that it needs to wait for all *N* data to be collected before processing and to improves the calculation speed. Meanwhile, when calculating DFT, it is necessary to compute the values of all *N* spectral lines. If only the amplitude and phase angle of a single frequency spectral line need to be calculated, the calculation of the remaining *N*-1 spectral lines will be wasted. From Formulas(18) and (19), it can be seen that Goertzel can only calculate the amplitude and phase angle of a specific spectral line, which also saves computational costs.

Preprints (www.preprints.org) | NOT PEER-REVIEWED | Posted: 23 May 2023 doi:10.20944/preprints202305.1623.v1

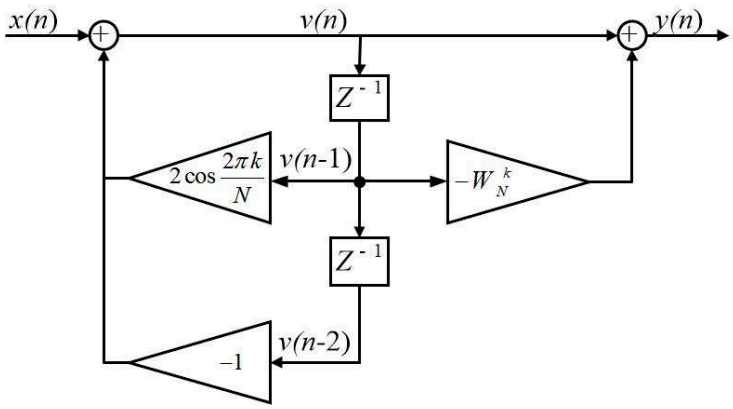

Figure 5. Goertzel algorithm flowchart.

4. Fault Features and Diagnostic Model of Traction Motor ITSC Fault

4.1. Fault Features of Traction Motor ITSC Diagnostic Conditions

When an ITSC fault occurs in a-phase winding of the traction motor, the symmetry relation of the three-phase winding changes. As shown in Figure 2, when diagnostic condition I is implemented while the traction motor is stationary, the b-phase and c-phase are in parallel. The inductance and resistance asymmetries exist between b-phase or c-phase winding due to an ITSC fault. The amplitude difference between the b-phaseand c-phase current Δi_{bc} will occur, and the phase angle difference $\Delta\theta_{bc}$ will also occur. Calculating the current amplitude difference Δi_{bc} and phase angle difference $\Delta\theta_{bc}$ between the b-phase and c-phase can detect the winding asymmetries caused by the ITSC fault on b-phase or c-phase winding. Similarly, diagnostic condition II can be applied to detect the asymmetries between the c-phase and a-phase; diagnostic condition III can be applied to detect the asymmetries between the a-phase and b-phase. Table 1 defines six ITSC fault diagnosis fault features under three diagnostic conditions when the traction motor is stationary.

Table 2. Definition of fault features.

Diagnostic condition I	Diagnostic condition II	Diagnostic condition III
$\Delta i_{bc}=i_{bmax}-i_{cmax}$	$\Delta i_{ca}=i_{cmax}-i_{amax}$	$\Delta i_{ab}=i_{amax}-i_{bmax}$
$\Delta\theta_{bc}=\theta_b-\theta_c$	$\Delta\theta_{ca}=\theta_c-\theta_a$	$\Delta\theta_{ab}=\theta_a-\theta_b$

4.2. Random Forest Fault Diagnosis Model

Random forest is a supervised ensemble learning algorithm based on decision trees. The random forest improves the performance of a single decision tree by random sampling with replacement using the Bootstrap method. It generates T train sets with no more samples than the original sample set. This method has been shown to improve the classification accuracy of the unstable classifiers [37-38]. T train sets are utilized to generate T decision trees. When the decision tree is split, a feature subset is randomly selected from all features with equal probability. A optimal feature splitting node is selected from it to make the classifier robust to noise and outliers. The voting method is used to select the category with the highest output from the T decision trees as the category to which the sample belongs. The algorithm flow of random forest is as follows [39-40]:

(1) The Bootstrap method is used to resample, and randomly select m samples from the original dataset with M samples and generate T train subsets, S_1, S_2,..., S_T. The number of train subset samples m should not be greater than M.

(2) The T train sets are used to generate T corresponding decision trees C_1, C_2, ..., C_T; before selecting features on each non-leaf node, s features are randomly selected from the S features as the split feature set for the current node and the node is split using the best splitting method among these s features.

Preprints (www.preprints.org) | NOT PEER-REVIEWED | Posted: 23 May 2023 doi:10.20944/preprints202305.1623.v1

(3) There is no restriction on the growth of each decision tree and no pruning;

(4) A random forest consisting of T decision trees is used to identify and classify the new data set, and the voting method is adopted. The final result is determined to the number of votes.

4.3. Fault Diagnosis of Traction Motor ITSC Fault

Figure 6 shows the ITSC fault flowchart for the traction motor stators based on the Goertzel algorithm and random forest. It mainly includes two parts: random forest model training and online diagnosis. In two parts, the fault diagnostic excitation SPWM voltage parameter setting and diagnostic condition control can be embedded in the EMU TCU control program. After training the ITSC fault diagnosis model, the TCU controls the inverter to perform three fault diagnostic conditions before the traction motor is driven. The current amplitude features Δi and phase angle features $\Delta\theta$ need to be calculated through Goertzel. The six fault features are input into the fault diagnosis model to diagnose the ITSC fault of the traction motor and output the diagnostic results. This diagnosis method can ensures that the traction motor is free of ITSC faults before the TCU controls the inverter to drive the traction motor.

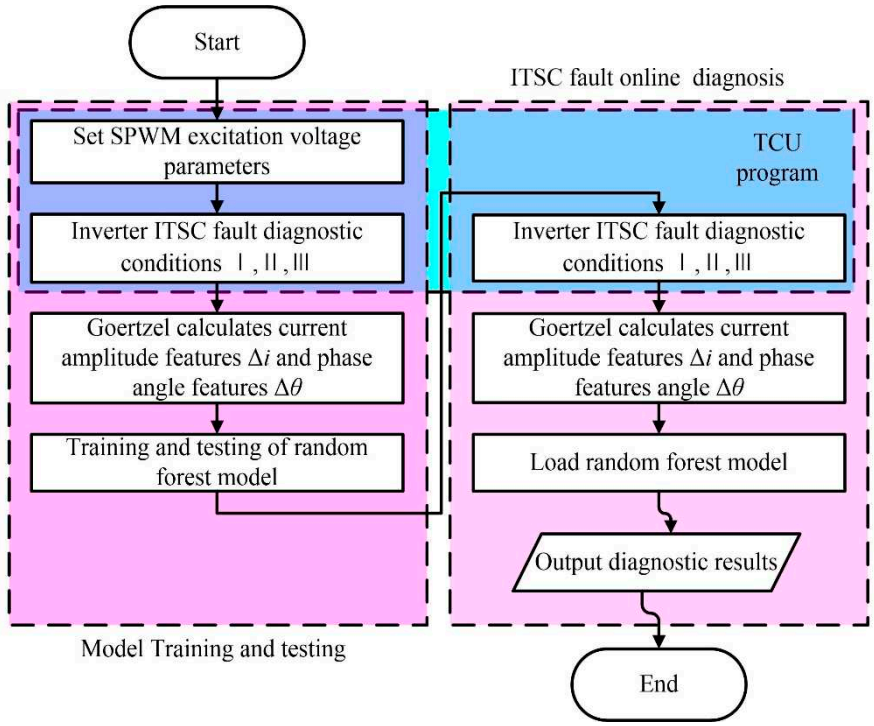

Figure 6. Flowchart of fault traction motor ITSC diagnosis.

5. Diagnosis For Traction Motor ITSC Fault Simulation Experimental Platform

5.1. Traction Motor ITSC Fault Diagnosis Simulation Experimental Platform

Figure 7 shows a schematic of the experimental simulation platform for the EMU's traction motor ITSC fault diagnosis. The fault diagnostic conditions control program on the PC was loaded into the DSP28335. The silicon rectifier equipment output a DC voltage to simulate the intermediate DC link voltage of the EMU. The power electronics development platform is composed of a DSP28335, IGBTs driver circuits, and a three-phase bridge inverter circuit. The power electronics development platform output the SPWM voltages required for the three diagnostic conditions. The ITSC fault simulation motor adopted a three-phase squirrel cage induction motor, and the three-phase winding tap was led to the junction box during fabrication, as shown in Figure 7. The metal short circuit fault was simulated by direct short-circuiting of connectors, and the non-metallic short circuit was simulated by connecting resistors between the connectors.

Preprints (www.preprints.org) | NOT PEER-REVIEWED | Posted: 23 May 2023 doi:10.20944/preprints202305.1623.v1

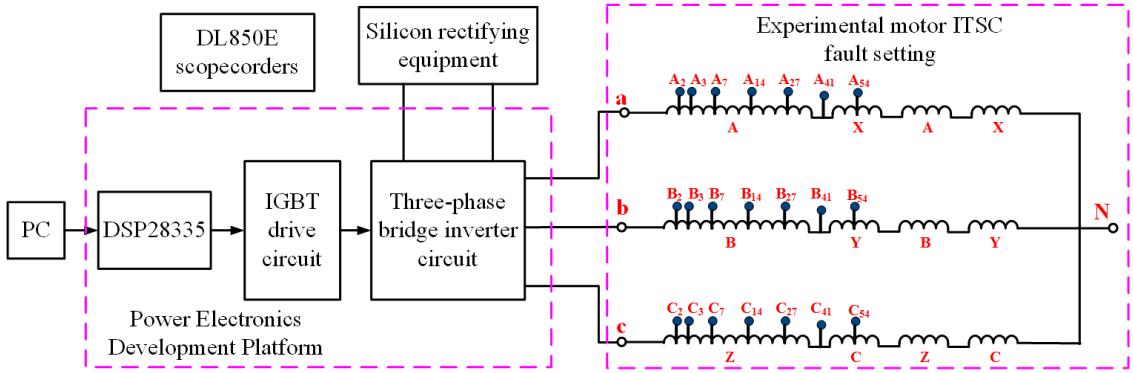

Figure 7. Traction motor ITSC fault diagnosis simulation experimental platform.

The real equipments of the ITSC fault diagnosis simulation experimental platform of the traction motor is shown in Figure 8. The voltage and current signals were measured using voltage and current probes, and a DL850E oscilloscope was used to store the voltage and current signals. During the experiment, the DC voltage, the motor phase voltage, the short-circuit inter-turn current, and the three-phase current were measured. The DL850E oscilloscope was used to collect and record the above signals. The DL850's LPF(low pass filter)was used for hardware filtering voltage and current signals. The LPF cutoff frequency was 400Hz. The sampling frequency f_s was set to 2000Hz for DL850E.

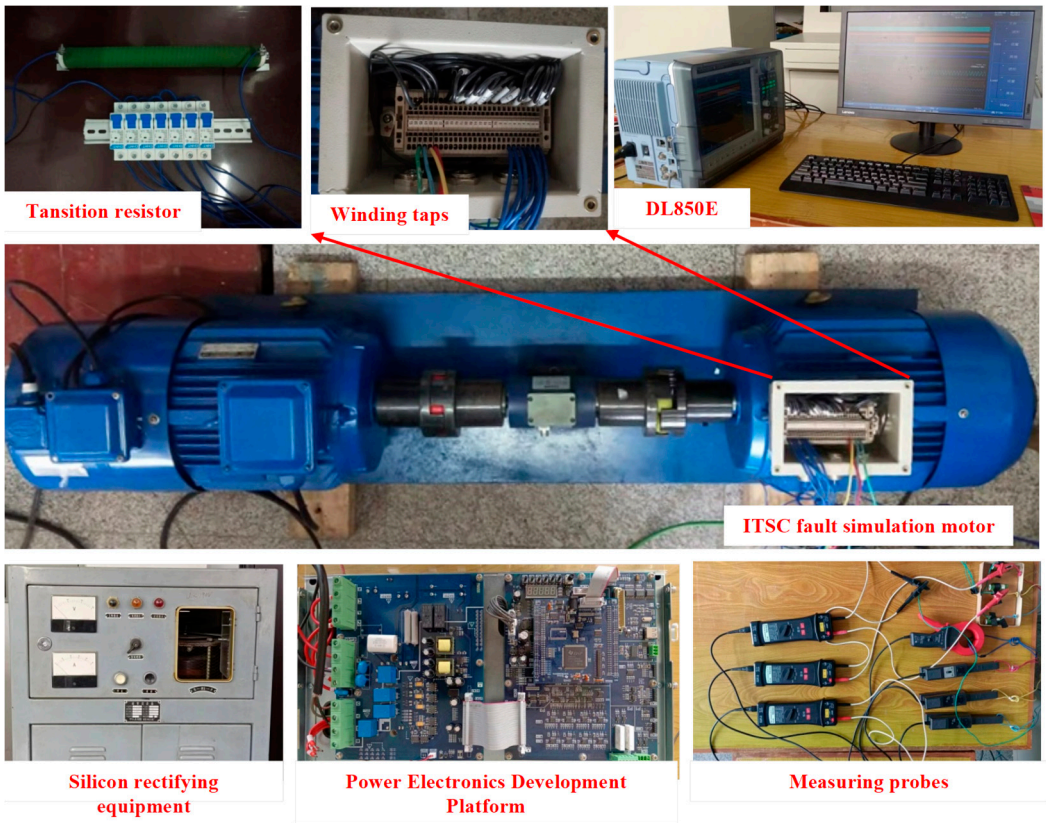

Figure 8. Photographs of the traction motor ITSC fault simulation experimental platform.

5.2. SPWM Excitation Voltage Parameters of Experimental Platform

The parameters of the ITSC fault experimental motor and the ITSC fault diagnosis control parameters are shown in Table 3. The silicon rectifier provided a DC300V voltage for the power electronics development platform. The SPWM reference modulation wave frequency f_r was 100Hz, the carrier frequency f_c was 5000Hz, and the modulation ratio N was 50. Considering both the ITSC

Preprints (www.preprints.org) | NOT PEER-REVIEWED | Posted: 23 May 2023 doi:10.20944/preprints202305.1623.v1

fault simulation motor nominal current and the power electronics development platform's output capability, the output current RMS value of the power electronics development platform was adjusted by changing the modulation index *M*. When the modulation index *M* was 0.4, RMS value of the equivalent parallel phase winding current of each diagnostic condition was about 3.5A, and the RMS value of the series winding current was about 7A.

Table 3. ITSC fault motor and diagnostic condition control parameters.

Parameters	Values	Parameters	Values
Nominal power	5.5kW	Nominal frequency	50Hz
Nominal voltage	380V	Connection mode	Y
Nominal current	11.7A	Nominal speed	1445rpm
Poles	4	Turns per phase	164
Modulation frequency	100Hz	Modulation index	0.4
Carrier frequency	5000Hz	DC-link voltage	300V

5.3. Analysis of ITSC Fault Diagnosis Signals

The measurement signals of a-phase ITSC fault with 1Ωtransition resistance and 39 short-circuit turns under diagnostic condition II were analyzed. Figure 9(a) shows the DC voltage waveform output by the silicon rectifier device. Figure 9(b) shows the motor phase voltage waveform after LPF filtering the SPWM voltage output from the power electronics development platform. The experimental induction motor phase voltages contain specific harmonic components. Under ITSC fault diagnostic condition II, as shown in Figure 3, the induction motor is equivalent to the a-phase winding in parallel with the c-phase winding and then connected in series with the b-phase winding. The phase voltage relationship is shown in Formula (20), and the waveforms of the a-phase voltage and the c-phase voltages in Figure 9(b) overlaps.

$$u_{an} = u_{cn} = -\frac{1}{2}u_{bn} \tag{20}$$

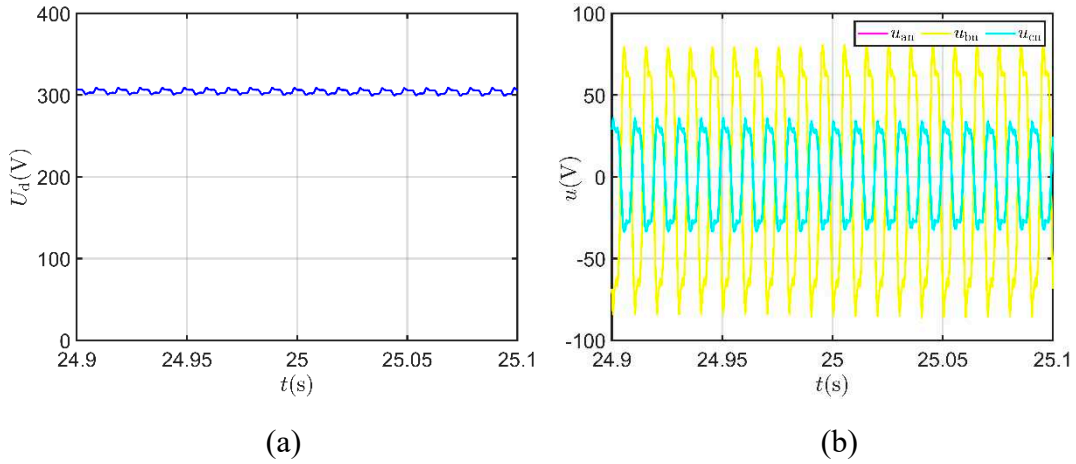

Figure 9. DC voltage and experimental motor phase voltages: (a) Output voltage of silicon rectifier equipment; (b) Diagnostic condition II experimental motor phase voltages.

Figure 10 (a) shows the short-circuit inter-turn current of the a-phase winding during an ITSC fault. After setting an ITSC fault in the a-phase, a sinusoidal current with a specific harmonic component is generated between the short-circuit turns. The DL850E trigger function was used to record the occurrence time of the short circuit faults, there was no ITSC fault in the a-phase before 24.99 seconds in recording time. Figure 10 (b) shows the three-phase current of the experimental motor with a fundamental frequency of 100Hz. When there is no ITSC fault, the phase current relation

Preprints (www.preprints.org) | NOT PEER-REVIEWED | Posted: 23 May 2023 doi:10.20944/preprints202305.1623.v1

of the experimental motor under ideal conditions is shown in Formula (21), i_a and i_c are almost equal, and their waveforms overlap. After the ITSC fault occurs in the a-phase, there is some difference between i_a and i_c, and their waveforms no longer overlap.

$$i_a = i_c = -\frac{1}{2} i_b \tag{21}$$

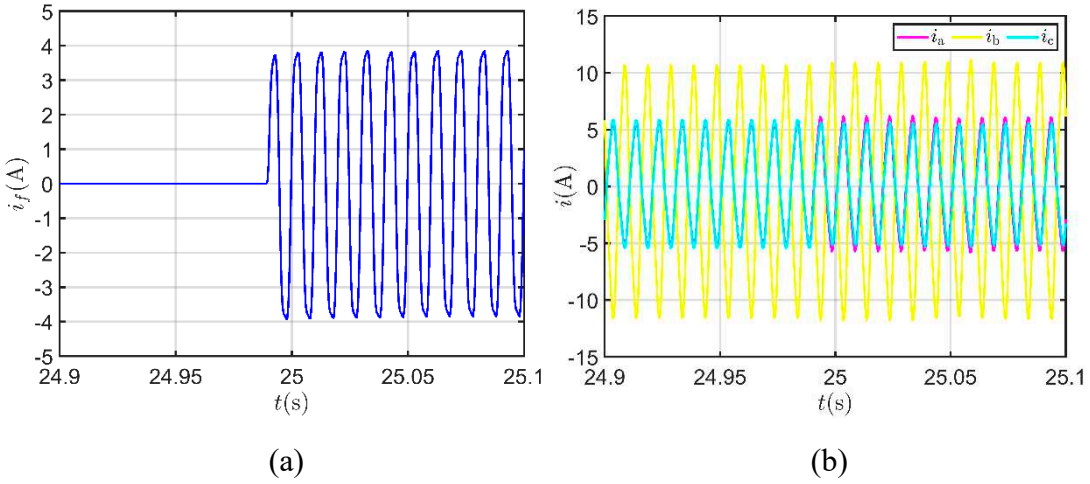

Figure 10. ITSC fault short-circuits inter-turn current and motor three-phase current: (a) ITSC fault short-circuit inter-turn current; (b) ITSC fault three-phase currents.

5.4. The Impact of ITSC Fault Extent on Features

The ITSC fault damage to induction motors is related to shout-circuit turns and transition resistance. Full period data truncation was used to eliminate the current fundamental frequency leakage. The Goertzel algorithm was used to calculate the six fault features under the three diagnostic conditions defined in Table 1. Table 4 shows the fault setting parameters during the experimental process. In the case of metal short- circuiting, the transition resistance value is 0. In the case of non-metallic short circuits, four resistance values were selected as the transition resistance. The second and seventh turns of each stator winding were used as the short-circuit ends. A total of 9 different short-circuit turns were obtained.

Table 4. ITSC fault setting parameters.

Parameters	values
Transition resistance (Ω)	0，1，2，4，8
Short-circuit turns	5，7，12，20，25，34，39，47，52

Figure 11 shows the variation of fault features with different numbers of short-circuit turns, the transition resistance of the experimental motor was 1Ω. Figure 11 (a) shows that after the ITSC fault occurs in the a-phase, Δi_{bc} feature remains almost unchanged with the change of short-circuit turns under diagnostic condition I. But, Δi_{ca} and Δi_{ab} significantly increases and decreases respectively with the increase of short-circuit turns under diagnostic condition II and III. Figure 11(b) shows that the $\Delta\theta_{bc}$ feature remains almost unchanged with the number of short-circuit turns under diagnostic condition I. But, $\Delta\theta_{ca}$ and $\Delta\theta_{ab}$ significantly increases and decreases respectively with the increase of short-circuit turns under diagnostic condition II and III.

Preprints (www.preprints.org) | NOT PEER-REVIEWED | Posted: 23 May 2023 doi:10.20944/preprints202305.1623.v1

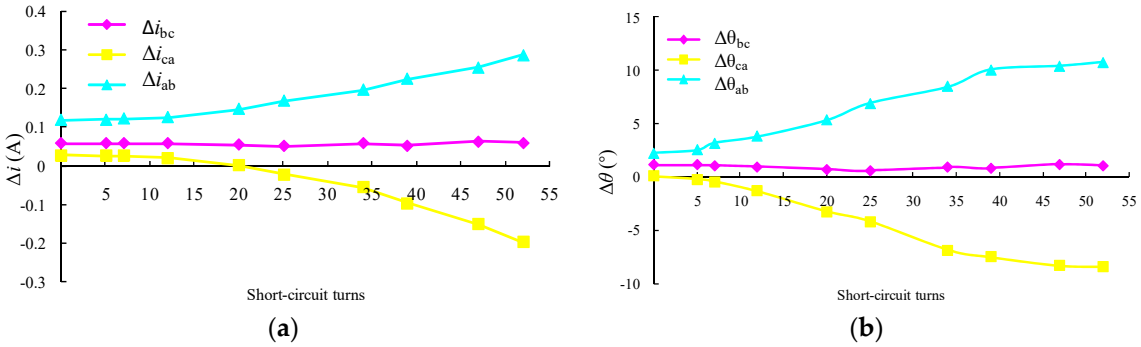

Figure 11. Current fault features change with different numbers of short-circuit turns: (a) Amplitude features Δi change with the numbers of short-circuit turns; (b) Phase angle features $\Delta\theta$ change with the numbers of short-circuit turns.

Figure 12 shows the fault features change with the transition resistance between short-circuit turns, the number of short-circuit turns was 39. Figure 12 (a) shows that after the ITSC fault occurs in the a-phase, Δi_{bc} feature remains almost unchanged with the change of the transition resistance under diagnostic condition I. But, Δi_{ca} and Δi_{ab} significantly increases and decreases respectively with the transition resistance increase under diagnostic condition II and III. Figure 12(b) shows that $\Delta\theta_{bc}$ feature remains almost unchanged with the transition resistance under diagnostic condition I. But, $\Delta\theta_{ca}$ and $\Delta\theta_{ab}$ significantly increases and decreases respectively with the increase of the transition resistance under diagnostic condition II and III.

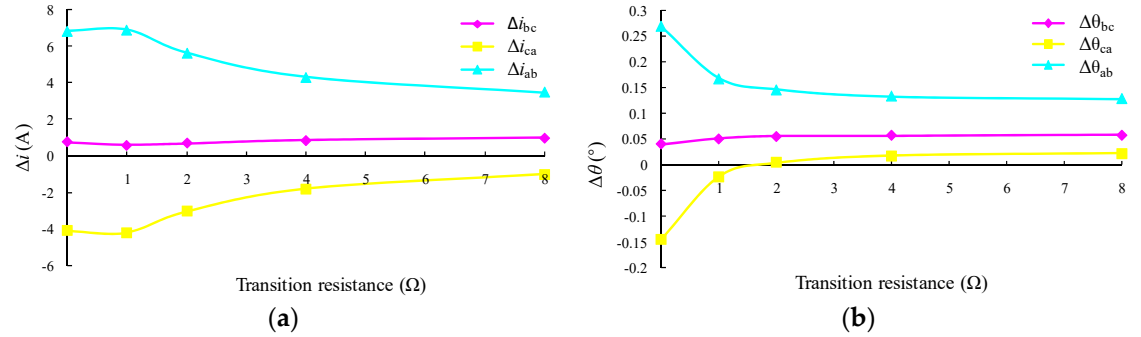

Figure 12. Current fault features change with the transition resistance: (**a**) Amplitude features Δi change with the transition resistance; (**b**) Phase angle features $\Delta\theta$ change with the transition resistance.

5.5. Fault Detection and Location Based on Random Forest Model

According to the fault experimental motor settings for ITSC simulation in Table 4, ITSC faults were set on each phase of the experimental motor. The six fault features as in Table 2 were measured and calculated. The train and test sets include 45 samples of ITSC faults at different extents in each phase and 45 healthy samples. A total of 180 samples were obtained in the experiment. The samples were labeled as healthy, a-phase ITSC fault, b-phase ITSC fault, and c-phase ITSC fault in the four types. Common machine learning algorithms were used to classify the data set and randomly selected 35 samples as train samples and 10 as test samples from various types. Table 5 shows that the various common classification algorithms have relatively high classification accuracy, indicating that the proposed fault feature extraction based on Goertzel algorithm for traction motors under the stationary state is effective. This method can provide reliable fault features for ITSC fault detection and location. In several common classification algorithms, random forest have a classification accuracy of 100% on both train and test samples. The ITSC fault can be accurately detected and located based on the Goertzel algorithm and the random forest for the ITSC fault simulation motor on the experimental platform . At the same time, the misclassified samples of the other classification

algorithms were analyzed, all of which were fault samples with high transition resistance and few short-circuited turns were misclassified as healthy samples.

Table 5. Diagnosis results of common classification models.

Models	Accuracy of the train sets	Accuracy of the test sets
BP neural network	97.86%	97.5%
KNN	98.57%	100%
SVM	95%	97.5%
Naive Bayes	99.29%	100%
Rondom Forest	100%	100%

6. Conclusions

This article proposes a method to control the traction inverter to output ITSC fault diagnostic SPWM excitation voltage under three different diagnostic conditions when the traction motor is stationary. According to the diagnostic condition control logic proposed in the article, the three-phase current under each diagnostic condition generates a pulsing magnetomotive force, which does not generate an electromagnetic torque. Based on the known fundamental frequency f_r of the excitation voltage for ITSC fault diagnosis, the Goertzel algorithm is used to calculate the fundamental current amplitude difference Δi and phase angle difference $\Delta\theta$ of the equivalent parallel windings under various diagnostic conditions. The amplitude difference Δi and phase angle difference $\Delta\theta$ under the three fault diagnostic conditions are used as fault features. The random forest is used as the ITSC fault diagnosis model. The above method was validated using a traction motor ITSC fault diagnosis simulation experimental platform. When the ITSC fault winding occurs in the equivalent parallel winding, the current amplitude difference Δi and phase angle difference $\Delta\theta$ were analyzed. The features changed significantly with the increase in fault extent. The ITSC fault diagnosis model based on the random forest was established with six fault features under three diagnostic conditions as input. The model can judge whether the experimental motor has an ITSC fault and locate the ITSC fault phase with 100% accuracy. The EMU traction motor ITSC fault diagnosis method proposed in the article is used before the motor starts, which can detect ITSC faults and ensure there are no ITSC faults before EMU start.

Author Contributions: Methodology, J.M., Y.L. ,J.F. and W.L. ; software, G.Z. and H.L.; validation, J.M.; formal analysis, J.M. and J.H.; investigation, G.Z.; resources, J.F.; data curation, J.M. and L.W. ; writing—original draft preparation, J.M, J.H. Y.L. and L.W.; writing—review and editing, J.F, H.L., L.L. and G.Z. ; visualization, L.L. and H.L. ; supervision, J.F and W.L . All authors have read and agreed to the published version of the manuscript.

Funding: This research was funded by the 2021 Scientific Research Fund Project of Liaoning Provincial Department of Education (LJKZ1297)".

Conflicts of Interest: The authors declare no conflict of interest.

References

1. Lee, S-G. A Study on Traction Motor Characteristic in EMU Train. In Proceedings of the 13th International Conference on Control, Automation and Systems, Gyeonggi-do, Korea, 22-25October 2014.
2. Chen, Z.P.; Wang, Z.; Jia, L.M.; Cai, G.Q. Analysis and Comparison of Locomotive Traction Motor Intelligent Fault Diagnosis Methods. *Appl. Mech. Mater.***2011**, *97–98*, 994–1002. doi:10.4028/www.scientific.net/AMM.97-98.994.
3. Chao, C.; Wang, W.; Chen, H.; Zhang, B.; Shao, J.; Teng, W. Enhanced Fault Diagnosis Using Broad Learning for Traction Systems in High-Speed Trains. *IEEE Trans. Power Electron.***2020**, *36*, 7461–7469. doi:10.1109/TPEL.2020.3043741.
4. Guo, X.; Tang, Y.; Wu, M.; Zhang, Z.; Yuan, J. FPGA-Based Hardware-in-the-Loop Real-Time Simulation Implementation for High-Speed Train Electrical Traction System. *IET Electr. Power Appl.***2020**, *14*,850-858.doi:10.1049/iet-epa.2019.0655.

5. Elbouchikhi,E.; Amirat, Y.; Feld, G.; Benbouzid, M. Generalized Likelihood Ratio Test Based Approach for Stator-Fault Detection in a PWM Inverter-Fed Induction Motor Drive. *IEEE Trans. Ind. Electron*.**2019**,*66*, 6343–6353.doi:10.1109/TIE.2018.2875665.
6. Al-Ameri, S.M.; Alawady, A.A.; Yousof, M.F.M.; Kamarudin, M.S.; Salem, A.A.; Abu-Siada, A.; Mosaad, M.I. Application of Frequency Response Analysis Method to Detect Short-Circuit Faults in Three-Phase Induction Motors. *Appl. Sci*.**2022**, *12*, 2046. doi:10.3390/app12042046.
7. Tallam, R.M.; Habetler, T.G.; Harley, R.G. Transient Model for Induction Machines With Stator Winding Turn Faults. *IEEE Trans. Ind. Appl*.**2002**, *38*, 632-637.
8. Kallesoe, C.S.; Vadstrup, P.; Rasmussen, H.; Izadi-Zamanabadi, R. Observer Based Estimation of Stator Winding Faults in Delta-Connected Induction Motors, a LMI Approach. In Proceedings of the IAS Annual Meeting, FL, USA , 08-12October2006.doi:10.1109/IAS.2006.256880.
9. Angelo, C.; Bossio, G.R.; Gi Ac Cone, S.J.; Valla, M.I.; Garcia, G.O. Online Model-Based Stator-Fault Detection and Identification in Induction Motors. *IEEE Trans. Ind. Electron*.**2009**, 56, 4671–4680. doi:10.1109/TIE.2009.2012468.
10. Nguyen, V.; Wang, D.; Seshadrinath, J.; Ukil, A.; Krishna, M.S.; Nadarajan, S.; Vaiyapuri, V. A Method for Incipient Interturn Fault Detection and Severity Estimation of Induction Motors Under Inherent Asymmetry and Voltage Imbalance. *IEEE Trans. Transp. Electrific*. **2017**, 3, 703–715. doi:10.1109/TTE.2017.2726351.
11. Abdallah, H.; Benatman, K. Stator Winding Inter-turn Short-circuit Detection in Induction Motors by Parameter Identification. *IET Electr. Power Appl*.**2017,***11*, 272–288. doi:10.1049/iet-epa.2016.0432.
12. Bachir, S.; Tnani, S.; Trigeassou, J.-C.; Champenois, G. Diagnosis by Parameter Estimation of Stator and Rotor Faults Occurring in Induction Machines. *IEEE Trans. Ind. Electron*. **2006**, 53, 963–973. doi:10.1109/TIE.2006.874258.
13. Bazine, I.B.A.; Tnani, S.; Poinot, T.; Champenois, G.; Jelassi, K. On-Line Detection of Stator and Rotor Faults Occurring in Induction Machine Diagnosis by Parameters Estimation. In Proceedings of the 8th IEEE Symposium on Diagnostics for Electrical Machines, Power Electronics & Drives; Bologna, Italy, 05-08September2011.doi:10.1109/DEMPED.2011.6063609.
14. Aswad, R.A.K.; Jassim, B.M.H. Detection and Localization of the Stator Winding Inter-Turn Fault in Induction Motors Based on Parameters Estimation Using Genetic Algorithm. *J. Inst. Eng. India Ser*. B **2022**, 103, 405–414. doi:10.1007/s40031-021-00670-x.
15. Nandi, S. Stator Fault Detection in Induction Machines Using Triplen Harmonics at Motor Terminal Voltage after Switch-Off. In Proceedings of the IEEE Power Engineering Society General Meeting, San Francisco, CA, USA, 12-16 June 2005.
16. Qing Wu; Nandi, S. Fast Single-Turn Sensitive Stator Interturn Fault Detection of Induction Machines Based on Positive- and Negative-Sequence Third Harmonic Components of Line Currents. *IEEE Trans. Ind. Appl*.**2010**,*46*,974–983. doi:10.1109/TIA.2010.2045329.
17. El Bouchikhi, E.H.; Choqueuse, V.; Benbouzid, M. Induction Machine Faults Detection Using Stator Current Parametric Spectral Estimation. *Mech Syst Signal Pr*.**2015**, 52–53, 447–464. doi:10.1016/j.ymssp.2014.06.015.
18. Ghanbari, T.; Samet, H. A Kalman Filter Based Technique for Stator Turn-Fault Detection of the Induction Motors. *Int.J.Emerg.Electr.P*.**2017**, 18,1-14. doi:10.1515/ijeeps-2017-0071.
19. Nazemi, M.H.; Gallehdar, D.; Haghjoo, F.; Cruz, S. A Secure and Sensitive Wavelet Transform Based Technique for Stator Fault Detection in the Cases of Line-connected and Inverter-fed Induction Machines. *IET Electr. Power Appl*.2021, 15, 1138–1153. doi:10.1049/elp2.12084.
20. Almounajjed, A.; Sahoo, A.K.; Kumar, M.K. Diagnosis of Stator Fault Severity in Induction Motor Based on Discrete Wavelet Analysis. *Measurement*. **2021**, *182*, 109780. doi:10.1016/j.measurement.2021.109780.
21. Lee, S.; Wang, Y.; Song, J. Fourier and Wavelet Transformations Application to Fault Detection of Induction Motor with Stator Current. *J. Cent. South Univ. Technol*. **2010**, 17, 93–101. doi:10.1007/s11771-010-0016-4.
22. Vinayak, B.A.; Varma, S.; Jagadanand, G. Precise Wavelet Selection for Condition Monitoring of Inverter-Fed Induction Machine. In Proceedings of the 2017 IEEE International Conference on Signal Processing, Informatics, Communication and Energy Systems (SPICES); Kollam, India, 08-10 August 2017.doi:10.1109/DEMPED.2011.6063609.
23. Seshadrinath, J.; Singh, B.; Panigrahi, B.K. Single-Turn Fault Detection in Induction Machine Using Complex-Wavelet-Based Method. *IEEE Trans. on Ind. Applica*t. **2012**, 48, 1846–1854. doi:10.1109/TIA.2012.2222012.
24. Akhil Vinayak, B.; Anjali Anand, K.; Jagadanand, G. Wavelet-based Real-time Stator Fault Detection of Inverter-fed Induction Motor. *IET Electr. Power Appl*.**2020**, *14*, 82–90. doi:10.1049/iet-epa.2019.0273.
25. Yang, J.; Huang, J.; Liu, T. Diagnosis of Stator Faults in Induction Motor Based on Zero Sequence Voltage after Switch-Off. *J. Zhejiang Univ. Sci. A***2008**, 9, 165–172. doi:10.1631/jzus.A071297.

26. Dash, R. N.; B. Subudhi.; S. Das. A comparison between MLP NN and RBF NN techniques for the detection of stator inter-turn fault of an induction motor.2010 International Conference on Industrial Electronics, Control and Robotics; Rourkela, India,27-29 December 2010.doi:10.1109/IECR.2010.5720163.
27. Mejia-Barron, A.; Tapia-Tinoco, G.; Razo-Hernandez, J.R.; Valtierra-Rodriguez, M.; Granados-Lieberman, D. A Neural Network-Based Model for MCSA of Inter-Turn Short-Circuit Faults in Induction Motors and Its Power Hardware in the Loop Simulation. *Comput.Electr.Eng*.**2021**, 93, 107234. doi:10.1016/j.compeleceng.2021.107234.
28. Yi, L.; Liu, Y.; Yu, W.; Zhao, J. A Novel Nonlinear Observer for Fault Diagnosis of Induction Motor. *J Algorithms.Comput.* 2020, 14, 174830262092272, doi:10.1177/1748302620922723.
29. Cherif, H.; Benakcha, A.; Laib, I.; Chehaidia, S.E.; Menacer, A.; Soudan, B.; Olabi, A.G. Early Detection and Localization of Stator Inter-Turn Faults Based on Discrete Wavelet Energy Ratio and Neural Networks in Induction Motor. *Energy*.**2020**, 212, 118684. doi:10.1016/j.energy.2020.118684.
30. Husari, F.; Seshadrinath, J. Incipient Interturn Fault Detection and Severity Evaluation in Electric Drive System Using Hybrid HCNN-SVM Based Model. *IEEE Trans. Ind. Inf.* **2022**, 18, 1823–1832. doi:10.1109/TII.2021.3067321.
31. Tian, R.; Chen, F.; Dong, S. Compound Fault Diagnosis of Stator Interturn Short Circuit and Air Gap Eccentricity Based on Random Forest and XGBoost. *Math. Probl. Eng*.**2021**,*42*, 2149048. doi：10.1155/2021/2149048.
32. Zhang, K.; Jiang, B.; Chen, F. Multiple-Model-Based Diagnosis of Multiple Faults With High-Speed Train Applications Using Second-Level Adaptation. *IEEE Trans. Ind. Electron.* **2021**, *68*, 6257–6266.doi:10.1109/TIE.2020.2994867.
33. Koodziejek, P.; D. Wachowiak. Fast Real-Time RDFT- and GDFT-Based Direct Fault Diagnosis of Induction Motor Drive.*Energies*.**2022**,15,1-7.
34. Sundararajan P; Sathik M; Sasongko F; et al. Condition Monitoring of DC-Link Capacitors Using Goertzel Algorithm for Failure Precursor Parameter and Temperature Estimation. *IEEE T.Power.Electr*, **2020**, 35(6),6386-6396.doi: 10.1109/TPEL.2019.2951859.
35. Papathanasopoulos, D.A.; Giannousakis, K.N.; Dermatas, E.S.; Mitronikas, E. D.Vibration monitoring for position sensor fault diagnosis in brushless dc motor drives. Energies, 14. Papathanasopoulos, D.A.;Giannousakis, K.N.; Dermatas, E.S.;Mitronikas, E.D. VibrationMonitoring for Position Sensor FaultDiagnosis in Brushless DC MotorDrives. *Energies***2021**, 14, 2248.doi: 10.3390/en14082248
36. Rafael Peña-Alzola; Michal Sztykiel; Catherine E. Jones; Patrick J. Norman; Gareth MooreJosep Pou; Graeme M. Bur. First-Fault Detection in DC Distribution With IT Grounding Based on Sliding Discrete Fourier-Transform. *IEEE Trans. Power Electron*. **2021**,36,3649-3654.doi:10.1109/TPEL.2020.3026985.
37. Prasetyo, Y.T. "The Big One"Earthquake PreparednessAssessment among Younger FilipinosUsing a Random Forest Classifier andan Artificial Neural Network.*Sustainability***2023**, 15, 679. doi:10.3390/su15010679.
38. Guo, G.; Cui, X.; Du, B.Random-Forest Machine LearningApproach for High-Speed RailwayTrack Slab Deformation IdentificationUsing Track-Side VibrationMonitoring. *Appl. Sci.* **2021**, 11, 4756. doi:10.3390/app11114756.
39. Liu, J.; Q. Y. Xu; W. S. Chen . Classification of Bird and Drone Targets Based on Motion Characteristics and Random Forest Model Using Surveillance Radar Data. *IEEE Access***2021**,9,160135-160144. doi:10.1109/ACCESS.2021.3130231.
40. Chen, S.; R. Yang; M. Zhong. Graph-based semi-supervised random forest for rotating machinery gearbox fault diagnosis. *Control.Eng.Pract*.**2021**,117,104952.doi:10.1016/j.conengprac.2021.104952.